

# An automated method for detection of layer activation order in information processing pathway of rat barrel cortex under mechanical whisker stimulation

Mufti Mahmud<sup>a,b</sup>, Elisabetta Pasqualotto<sup>a</sup>, Alessandra Bertoldo<sup>b</sup>, Stefano Girardi<sup>a</sup>, Marta Maschietto<sup>a</sup>, Stefano Vassanelli<sup>\*,a</sup>

<sup>a</sup>*NeuroChip Laboratory, Department of Human Anatomy and Physiology, University of Padova, via f. Marzolo 3, 35131 Padova, Italy*

<sup>b</sup>*Department of Information Engineering, University of Padova, via Gradenigo 6/B, 35131 Padova, Italy*

---

## Abstract

Rodents perform object localization, texture and shape discrimination very precisely through whisking. During whisking, microcircuits in corresponding barrel columns get activated to segregate and integrate tactile information through the information processing pathway. Sensory signals are projected through the brainstem and thalamus to the corresponding ‘barrel columns’ where different cortical layers are activated during signal projection. Therefore, having precise information about the layer activation order is desirable to better understand this signal processing pathway. This work proposes an automated, computationally efficient and easy to implement method to determine the cortical layer activation from intracortically recorded local field potentials (LFPs) and derived current source density (CSD) profiles:

1. Barrel cortex LFPs are represented by a template of four subsequent events: small positive/negative (E1)→large negative (E2)→slow positive (E3)→slow long negative (E4). The method exploits the layer specific characteristics of LFPs to obtain latencies of the individual events (E1–E4), then taking the latency of E2 for calculating the layer activation order.

2. The corresponding CSD profile is calculated from the LFPs and the first sink’s peak is considered as a reference point to calculate latencies and evaluate the layer activation order. Other reference points require manual

---

\*Corresponding author. Tel.: +39 049 8275337; fax: +39 049 8275301.

*Email address:* stefano.vassanelli@unipd.it (Stefano Vassanelli)

calculation.

Similar results of layer activation sequence are found using LFPs and CSDs. Extensive tests on LFPs recorded using standard borosilicate micropipettes demonstrated the method's workability. An interpretation of layer activation order and CSD profiles on the basis of a simplified interacortical barrel column architecture is also provided.

*Key words:* Layer activation order, barrel cortex, whisker stimulation, local field potentials, current source density.

---

## 1. Introduction

To explain brain activity underlying perception as the outcome of elementary neuronal responses is one of the major challenges of sensory systems neuroscience. Through “whisking”, rodents make extremely fine discriminations of the environment, e.g., object localization, basing on shapes and textures of the objects (Ahissar and Knusten, 2008). The mammal cortex shows a high degree of areal and laminar differentiation and also a representation of sensory surfaces. Especially for the rodents there is a precise topological map of the mystacial pad in the S1 cortex, in which for each whisker there is a so called “barrel” that receives the tactile information (Diamond et al., 2008). Barrels play a very important role in segregation, integration and transmission of sensory information as sensory innervations at each whisker follicle are numerous (larger follicles receives terminations from approximately 200 trigeminal ganglion cells and the smaller follicles about 50) (Fox, 2008). During transmission of the information different layers of the barrel cortex are activated at different times. Studies have shown that intra- and transcolumar microcircuits in the barrel cortex segregate and integrate information during this activation (Schubert et al., 2007) and that these microcircuits have specific understanding of ‘what’, ‘where’ and ‘when’ aspects of the tactile information acquired by the whiskers.

To have precise knowledge about this information processing pathway by means of extracellular recording and offline signal analysis, an automated, reliable, and quick method is required. Indeed, scientists commonly perform this work manually spending lot of time especially when signals are recorded using neural probes with multiple recording sites.

In this work, we present an automated, simple to implement and computationally efficient method (computational complexity  $O(n^2)$ ) capable of

28 detecting various events (E1–E4) that characterize the LFPs recorded from  
29 different layers of the barrel cortex upon mechanical whisker stimulation.  
30 Latencies of the different events from the stimulus–onset are determined and  
31 the activation order of the cortical layers is calculated using the latency of  
32 E2 (i.e. the highest negative peak).

33 Generally, however, scientists determine the cortical layer activation or-  
34 der based on the current flow through the cortical layers by calculating the  
35 current source density corresponding to the LFPs. Therefore, this analysis  
36 is also implemented in the program, thus allowing for automated calcula-  
37 tion of the layer activation order from CSDs obtained using the  $\delta$ -source  
38 inverse current source density ( $\delta$ -Source iCSD) method (Pettersen et al.,  
39 2006). The program first calculates the latency of the first sink’s peak from  
40 the stimulus–onset of each CSD, then it groups the recordings layerwise and  
41 stores the minimum latencies corresponding to each layer in an increasingly  
42 ordered list. The layer activation order is determined automatically by tak-  
43 ing the minimum latency of each layer. The program was tested on LFPs  
44 measured from the rat barrel cortex under whisker stimulation. Resulting  
45 CSDs and layer activation order were comparable with previously recorded  
46 data (Jellema et al., 2004) and compatible with the intracortical network  
47 architecture of the barrel cortex (Fox, 2008). We found that the activation  
48 order estimated using the LFPs and CSDs are similar. Also, automated re-  
49 sults on layer activation order using LFPs were supported by an in-depth  
50 manual analysis of the same data samples.

## 51 **2. Signal acquisition**

### 52 *2.1. Animal preparation*

53 Wistar rats were maintained in the Animal Research Facility of the De-  
54 partment of Human Anatomy and Physiology (University of Padova, Italy)  
55 under standard environmental conditions.

56 P30-P40 male rats were anesthetized with an induction mixture of Tile-  
57 tamine (2 mg/100 g weight) and Xylazine (1.4 g/100 g weight). The anes-  
58 thesia level was monitored throughout the experiment by testing eye and  
59 hind-limb reflexes, respiration and checking the absence of whiskers’ sponta-  
60 neous movements. Whenever necessary, additional doses of Tiletamine (0.5  
61 mg/100 g weight) and Xylazine (0.5 g/100 g weight) were provided.

62 During the surgery and the recording section, animals were kept on a  
63 common stereotaxic apparatus under a stereomicroscope and fixed by teeth

64 and ear bars. The body temperature was constantly monitored with a rectal  
65 probe and maintained at about 37° C using a homeothermic heating pad.  
66 Heart beat was assessed by standard ECG. To expose the cortical area of  
67 interest, anterior-posterior opening in the skin was made along the medial  
68 line of the head, starting from the imaginary eyeline and ending at the neck.  
69 While the skin was kept apart using halsted-mosquito hemostats forceps, the  
70 connective tissue between skin and skull was gently removed by means of a  
71 bone scraper. Thus, the skull over the right hemisphere was drilled to open  
72 a window in correspondence of the somatosensory cortex, S1 ( $-1 \div -4$  AP,  
73  $+4 \div +8$  ML) (Swanson, 2003). Meninges were then carefully cut by means  
74 of forceps at coordinates  $-2.5$  AP,  $+6$  LM for the subsequent insertion of the  
75 recording micropipette.

76 Throughout all surgical operations and recordings, the brain was bathed  
77 by a standard Krebs solution (in mM: NaCl-120, KCl-1.99, NaHCO<sub>3</sub>-25.56,  
78 KH<sub>2</sub>PO<sub>4</sub>-136.09, CaCl<sub>2</sub>-2, MgSO<sub>4</sub>-1.2, glucose-11), constantly oxygenated  
79 and warmed at 37° C.

80 At the end of the surgery, contralateral whiskers were trimmed at about  
81 10 mm from the mystacial pad.

## 82 *2.2. Whisker stimulation and recording*

83 The recording of LFPs from S1 was performed by means of borosilicate  
84 micropipettes (1 MΩ resistance), filled with Krebs solution. The pipette was  
85 fixed to a micromanipulator so that it was 45° tilted with respect to the  
86 vertical axis of the manipulator, thus being inserted perpendicularly to S1  
87 cortex surface. The figure 1 depicts the experimental setup and the stimulus  
88 waveform used in driving the stimulator.

89 LFPs were evoked by single whiskers mechanical stimulation performed  
90 with a custom-made speaker that provides dorsal-ventral movements through  
91 a connected tube. The speaker was driven by a waveform generator (Agilent  
92 33250A 80 MHz, Agilent Technologies) providing 1 ms, 10 V square stimuli  
93 with 150 ms delay. Each whisker, starting from the posterior group, was in-  
94 dividually inserted into the tube and the corresponding response was checked  
95 at  $-750 \mu\text{m}$  depth (cortical layer IV), in order to find the most responsive  
96 whisker for the selected recording point in the cortex. The so-called “princi-  
97 pal whisker” was then chosen for the recording, and the evoked LFPs were  
98 recorded from all the cortical layers with a  $90 \mu\text{m}$  recording pitch. For each  
99 depth, 100 sweeps with 500 ms duration are recorded at 20 kHz sampling  
100 rate. An open source software, ‘WinWCP’ (Version: 4.1.0) developed by the

101 SIPBS, University of Strathclyde, UK ([http://spider.science.strath.](http://spider.science.strath.ac.uk/sipbs/software_ses.htm)  
102 [ac.uk/sipbs/software\\_ses.htm](http://spider.science.strath.ac.uk/sipbs/software_ses.htm)) was used for recording the signals.

Figure 1: Experimental setup depicting its various components. The arrow on the metal tube connected to the stimulator shows the direction of its movement. Bottom is the stimulus waveform used in driving the speaker, causing dorsal-ventral movement of whisker that is inserted in the metal tube.

### 103 2.3. *The signals*

104 The LFPs recorded from a barrel column of the rat S1 cortex by stimulat-  
105 ing the corresponding whisker can be differentiated by their specific charac-  
106 teristics based on the depth or layer they are recorded from. Figure 2 shows  
107 a representative depth profile of one of our experiments.

108 As illustrated in (Ahrens and Kleinfeld, 2004; Kublik, 2004), usually in  
109 upper cortical layers (I, II) the signals are expected to have a small positive  
110 peak, followed by a main negative peak, a positive peak and a slow negative  
111 valley that gradually tends to reach the baseline at the end. In the middle  
112 layers (III, IV, and V) the signals are expected to have the main negative  
113 peak (without the first small positive peak) followed by a slow positive peak  
114 and a slow negative valley tending to reach zero at the end. Deep in the  
115 cortex (layer VI), the main negative peak becomes smaller and usually gets  
116 divided into two smaller negative peaks, followed by a slow positive peak  
117 and then the slow negative valley. These characteristics of the signals can be  
118 exploited in automated detection of the layers from the recorded signals.

Figure 2: Depth profile of local field potentials recorded from the E1 barrel column by stimulating the E1 whisker where the different features of the signals can be easily seen. The full depth profile contained equidistant recordings spaced by  $90 \mu m$ , but for the ease of visualization only representative signals from each layer are shown.

## 119 3. Method

### 120 3.1. *Determining cortical layer activation order directly from LFPs*

121 This method is implemented using the MATLAB ([http://www.mathworks.](http://www.mathworks.com)  
122 [com](http://www.mathworks.com)) scripting with an easy to use Graphical User Interface (GUI). The figure  
123 3 shows the GUI that encapsulates the implementation for the ease of use of  
124 the non-programming background users. The figure 4 shows the flowchart  
125 of its basic operational steps (Mahmud et al., 2010a).

Figure 3: GUI of the layer activation order calculation method using LFPs. This GUI provides an easy way for the non-programming background users to use the method in analyzing their data obtained from experiments.

126 The method takes the signal files recorded from the rat barrel cortex upon  
127 whisker stimulation as input. For each file it calls a module (the flowchart  
128 of the module is shown in figure 5) capable of detecting the events present  
129 in that signal and calculating the latencies from the starting of the evoked  
130 response.

Figure 4: Flowchart showing the operational steps of the layer activation detection method using LFPs.

131 The layer of recording is determined basing on a priori information about  
132 the recording depths of the LFPs. Finally the activation order of different  
133 cortical layers in the barrel column is determined by sorting the layerwise  
134 minimum latencies of the second event (E2).

135 The flowchart of the module used in detection of events and calculation  
136 of latencies is shown in figure 5. In this module, firstly the signal is low-pass  
137 filtered with 250 Hz cutoff frequency and is translated by setting the signal  
138 amplitude at the stimulus-onset to zero. This translation helps in avoiding  
139 the slow deviation of signal that might obscure the real amplitude of the  
140 events. The calculation of the latencies is based on the detection of various  
141 signal events (see Sec. 2.3) by calculating signal derivatives. A major change  
142 in the derivative is used in detecting an event.

Figure 5: Flowchart of the event detection and latency calculation module.

143 The event detection starts with the detection of the response-onset, which  
144 is considered as the starting point of the evoked response. To detect the exact  
145 response-onset, the standard deviation of the signal's steady-state (the signal  
146 before the stimulus-onset) is calculated. The signal from the stimulus-onset  
147 to the next 10 ms is divided into very small parts (0.5 ms duration), and  
148 derivatives of these parts are calculated. The response-onset is the time  
149 instance of the signal when a small part's derivative is found to exceed  $\pm$   
150 standard deviation of the steady-state.

151 The events are time locked, which means that a change in the signal  
152 derivative in a particular time window (either from up to down or vice versa)

153 denotes a particular event. Thus, dividing the signal (from the response–  
154 onset till the end of the signal) into smaller parts and then scanning for  
155 change of derivative is used in detecting event occurrences.

156 Special care is taken in case of the E1, which may or may not be present  
157 in a signal and if present, may have either positive or negative direction. In  
158 case of the positive E1, a threshold of 10  $\mu\text{V}$  is set to make sure that it indeed  
159 is an event and not just background spontaneous brain activity. If the signal  
160 is found to be going down, then the maximum negative peak is found and  
161 from this peak the signal ranging  $\pm 5$  ms is scanned for occurrence of yet  
162 another negative peak. If this second negative peak is found, the E1 is set  
163 as the first occurring negative peak and the E2 is the second negative peak,  
164 otherwise, the E1 is absent and the E2 is the maximum negative peak.

165 The detection of the rest of the events is very straightforward. It has  
166 been empirically found that the next event (E3, i.e., slow positive peak)  
167 occurs within the next 100 ms of the second event and the last event (E4,  
168 i.e., slow negative valley) within the 200 ms of the previous event.

169 Once the events (E1–E4) are detected, latencies are calculated by sub-  
170 tracting the occurrence time of these events from the stimulus–onset time.  
171 The signal characteristics and the latencies are saved in a file for further  
172 processing.

173 After the latencies are calculated for all signal files, they are assigned to  
174 the cortical layers from where the signals were recorded from basing on a  
175 priori position information. Minimum latencies associated to each layer are  
176 then found and sorted in ascending order to determine the order of cortical  
177 layers activation.

### 178 3.2. Determining cortical layer activation order using CSD

179 Due to the widespread use of current source density (CSD) analysis to  
180 obtain the layer activation order, we implemented also this approach in our  
181 program. To calculate the CSDs, we considered the  $\delta$ –Source Inverse CSD  
182 method ( $\delta$ –source iCSD) as explained in the next subsection. Figure 6 shows  
183 the MATLAB graphical user interface that generates the CSD profile from  
184 the LFPs and calculates the layer activation order.

Figure 6: GUI of the layer activation order calculation method using CSDs.

185 *3.2.1. The  $\delta$ -Source iCSD method*

186 The method, which has been adopted from Pettersen et al. (Pettersen et  
 187 al., 2006), divides the cortex to infinitely thin current discs each of radius  $R$   
 188 with constant planar CSD,  $C_p$ . For every recording site there is a disc with  
 189 a determined  $C_p$  that lies in the  $xy$  plane. In this way, we have a  $\delta$  function  
 190 in the  $z$ -direction, whose value is  $C_p$  at the recording site and zero between  
 191 two consecutive recording sites. The potential  $\phi(z)$  at the center of a disc  
 192 positioned at the position  $z'$  with recording pitch of  $h$  is given by:

$$\phi(z, z') = \frac{h}{2\sigma} (\sqrt{(z - z')^2 + R^2} - |z - z'|) C \quad (1)$$

193 where  $C = C_p/h$  is the equivalent volume CSD, that corresponds to the  
 194 CSD obtained if the planar current was distributed in a box of height  $h$   
 195 in which the disc is embedded and  $\sigma$  is the conductivity tensor in the rat  
 196 brain (default value is considered as 0.42 S/m as experimentally reported by  
 197 Sekino and Ohsaki, 2009). It is assumed that potential at position  $z_j$  is due  
 198 to the sum of contributions from the various discs positioned at the recording  
 199 electrode's contact points, and can be calculated using:

$$\phi(z_j) = \sum_N^{i=1} \left[ \frac{h}{2\sigma} (\sqrt{(z_j - z_i)^2 + R^2} - |z_j - z_i|) \right] C(z_i) \quad (2)$$

$$= \sum_N^{i=1} F_{ji} C(z_i) \quad (3)$$

200 where  $F$  is an  $N \times N$  matrix, denoting that from  $N$  values of LFPs we  
 201 obtain  $N$  values of CSD. Furthermore, the elements of  $F$  are affected by the  
 202 appropriate value of the current disc's radius ( $R$ ) (experimentally reported  
 203 values are: 300  $\mu\text{m}$  and 200  $\mu\text{m}$  by Brett-Green et al., 2001 and Alloway,  
 204 2008, respectively; default value for the method is considered to be 250  $\mu\text{m}$ )  
 205 and are given by:

$$F_{ji} = \frac{h}{2\sigma} (\sqrt{(z_j - z_i)^2 + R^2} - |z_j - z_i|) \quad (4)$$

206 Now the CSD profiles can be estimated by inverting the matrix  $F$  and  
 207 multiplying with the calculated potentials at various recording positions:

$$\hat{C} = F^{-1}\phi \quad (5)$$

208 *3.2.2. Preprocessing*

209 Before applying the CSD analysis, raw LFPs are low-pass filtered using  
210 a Butterworth filter with cutoff frequency of 250 Hz. This is done to remove  
211 the high frequency components present in the LFPs that would cause un-  
212 expected oscillations in the calculated CSD profile. Moreover, resolution of  
213 CSD calculation depends on the recording pitch, with resolution improving  
214 by reducing the pitch. Therefore, to facilitate calculation of CSDs with large  
215 recording pitches, often interpolation of LFPs is performed (Rappelsberger  
216 et al., 1981). During higher order interpolation high spatial frequency noise  
217 occurs especially in the neighborhood of the boundary points. To reduce  
218 this high spatial frequency noise a symmetrical, weighted average of the LFP  
219 about a given point is applied with the form of equation 6 (Hamming filter)  
220 (Szymanski et al., 2009; Ulbert et al., 2001).

221 For signals recorded using neural probes with multiple recording sites  
222 separated by a small pitch (simultaneous recording producing a depth profile)  
223 the Hamming filter is not necessary. However, it may be applied for removing  
224 spatial noise (if any) present in the recordings. In situations where recording  
225 is done at different times at different sites (using micropipettes or any other  
226 extracellular electrode), Hamming filtering is applied under the assumption  
227 that the physiological response of the animal and the stimulus do not change  
228 during the recording session, i.e., the response to the stimulus at a specific  
229 depth is reproducible over the whole experiment.

$$\phi(z) = 0.23\phi(z - h) + 0.54\phi(z) + 0.23\phi(z + h) \quad (6)$$

230 After applying the Hamming filter only  $N - 2$  interior recordings can be  
231 considered excluding the first and last recordings.

232 *3.2.3. Detection of layer activation order using CSD*

233 After the CSD profile is computed, the sources and sinks for the individual  
234 recording site can easily be viewed. The calculation of the sinks' latencies is  
235 done by subtracting the time instance of the stimulus-onset from the time  
236 instance of the peak of the first sink.

237 Once the latencies are calculated for the whole CSD profile, recordings for  
238 each layer are grouped together and the minimum latencies are selected. To  
239 determine the layer activation order, minimum latencies are sorted in ascend-  
240 ing order and assigned to the different layers depending on recording depths  
241 known a priori. Latencies can be used to gain information on signal prop-  
242 agation within intracortical networks. Representative LFPs recorded from

243 the rat barrel cortex under whisker stimulation and corresponding CSDs  
244 computed by the program are shown as an example in figure 7 (A, B). Hypo-  
245 theoretical signal propagation pathways across the barrel intracortical network  
246 are inferred from the CSD profile and the latencies temporal pattern (as seen  
247 in figure 7 (C)) (Fox, 2008; Jellema et al., 2004).

248 To verify the activation order, sinks are shaded and along with sources  
249 they are annotated (as seen in figure 7 (B)), and a plausible neuronal network  
250 architecture corresponding to the CSD profile is drawn in figure 7 (C) for  
251 explanatory purpose. This hypothetical network architecture simply reflects  
252 the current flows that are seen by the sinks and sources in the calculated  
253 CSD profile.

254 Latencies indicated that the signals propagated through a pathway start-  
255 ing from Vb and then traversing through Va, III, IV, II, I and to VI. This  
256 order of layer activation is supported by the known neuronal architecture of  
257 the barrel cortical layers. This architecture suggests that the thalamic inputs  
258 (VPM) activate the layer Vb/IV, signals propagate through layer III and II  
259 from where the outputs are projected to layer Va, Vb. From these layers the  
260 output is sent to the layer VI and then back to the thalamus.

Figure 7: (A): Depth profile of recorded LFPs. (B): The respective CSD profile computed using  $\delta$ -source iCSD from the LFPs. The hatched portions of the profile denote the sinks (a-l) and the negative portions the sources (1-10). Stars indicate the initiation sites of the current flow within the cortex. (C): Barrel column architecture derived from previous studies (Fox, 2008; Jellema et al., 2004) showing the possible connections among neurons in different cortical layers. Arrows indicate either signal propagation (alphabet-to-alphabet: propagation of sinks; number-to-number: propagation of sources) or directed inward current (number-to-alphabet: current flow from source to sink) according to the nomenclature adapted by (Jellema et al., 2004). From the analysis of the CSD profile and latencies it is inferred that, there are two dominant sink-source complexes. The first one is initiated at the upper part of layer Va (sink 'a') and ending at layer I (sink 'f'); the second one is initiated at the lower part of layer Vb (sink 'g') and ending at layer VI (sink 'l'). The two complexes are assumed to be caused by the monosynaptic thalamic input (Fox, 2008) and are initiated through the sinks 'a' and 'g' after whisker stimulation. The first complex is supposed to be initiated by the pyramidal cells situated in the upper part of layer Va. This complex is propagated through neurons in the layer IV, III, and II. The axons of these cells are projected towards layer III (in case of Va) and layer I (in case of IV, III, and II). Propagation of this complex created huge sinks (sinks 'a' to 'f' in the CSD profile) and sources (1, 4, 3, and 6). The second complex is supposed to be initiated by pyramidal cells situated in the lower part of layer Vb and propagated through the lower portion of layer Va. During this propagation sinks 'g' to 'k' with increasing amplitude are generated. Indeed, the sink 'g' at the beginning of propagation is relatively small. Afterwards, sinks increase in amplitude and width possibly due to the fact that pyramidal cells involved in propagation receive other excitatory inputs from layer IV. Sources 2, 5, 7, 8, and 9 are associated to sinks 'g', 'h', 'i', 'j', 'c' and 'k', respectively. In layer VI and deeper polysynaptic delayed inputs caused additional sinks (sinks 'l'). Wires represent schematically excitatory connections.

Figure 8: Simplified architecture of a barrel column as described in (Fox, 2008). When a whisker is stimulated, the information first goes to the thalamus, and then from the thalamus to the corresponding barrel. As it can be seen from the picture, there are two principal thalamic inputs (VPM) that are in layer IV and at the border between layers Vb and VI. The thalamic inputs in layer IV activate both excitatory (represented by stellate cells) and inhibitory cells (represented by basket cells). These basket cells provide feedforward perisomatic inhibition from the VPM and feedback inhibition to the excitatory stellate cells. The LTS (low threshold spike) cells do not receive a thalamic input directly, so they are involved only in the feedback inhibition. The excitatory output from here is then projected to layers II/III. It should be noted that there are connections between inhibitory cells, in order to increase inhibition, and between the excitatory cells themselves. From the literature, it is known that stellate cells connect mainly with other stellate cells and pyramidal cells with other pyramidal cells. The excitatory cells of the granular layer (IV) then project to the supragranular layers (II/III). The connections between layer IV and layers II/III are numerous and strong, which may reflect the large amplitude of the sinks in these regions. Even in this case, basket cells provide both feedforward and feedback inhibition as the chandelier cells project to the axon initial segment of pyramidal cells. The excitatory outputs from these pyramidal cells are projected to layers V/VI. The output of the supragranular layers becomes the input for the infragranular layers, i.e., layers II–Va and III–Vb reciprocally connect within a column. Pyramidal cells of layers V and VI can be inhibited by inhibitory cells of same or other layers, such as the Martinotti cells. Sensory information finally reaches layer VI, whose cells are reciprocally connected with layer Vb cells, and from there comes back to the thalamus. From the picture it can be noted that layer IV connects also with layer Va and VI cells. The dash-dot-dashed and dashed lines are the feedback connections that project from the layer Vb back to layer III and from the layer VI back to the inhibitory cells of layer IV, respectively.

261     A simplified architecture of a barrel column reconstructed from (Fox,  
262 2008) is depicted in figure 8. Signal propagation estimated from CSD analysis  
263 matches, to a certain extent, the pathway through the single barrel. Of  
264 course, as the dynamics of individual events involved in signal generation  
265 and propagation through the network is largely unknown, the predictive  
266 potential of this network model regarding circuit activation remains limited.

### 267 3.3. Manual calculation of cortical layer activation

268     As a proof of automated detection reliability, the layer activation or-  
269 der was also calculated manually from the LFP profile. Latencies from  
270 the stimulus-onset were estimated manually for each event (E1–E4) using  
271 a commercial software (clampfit, v.10.0, <http://www.moleculardevices.com/Products/Software/Electrophysiology/pCLAMP.html>). This software  
272 provides time instance and amplitude of the signal's data point where the  
273 data-cursor was placed. Thus, the events were pointed manually one-by-one  
274

275 and the time instances noted. The latencies of the events were calculated by  
276 subtracting the stimulus-onset from the time instance of each event. Again,  
277 only E2 latencies were considered for calculation of the layer activation order.  
278 Then, E2 latencies were grouped layerwise and the minimum latency in each  
279 layer was found. These minimum latencies were then sorted in ascending  
280 order to determine the signal propagation among the layers. A comparison  
281 between automated and manual detection results is shown in the Results and  
282 discussion section.

## 283 4. Results and discussion

284 The event detection algorithm described in section 3.1 has a computa-  
285 tional complexity of  $O(n^2)$ . Another method proposed for event detection  
286 in LFPs (Bokil et al., 2006) was based on an algorithm with higher com-  
287 putational complexity  $O(\log n!)$ . Furthermore, algorithms used to detect  
288 PQRST complexes in ECG signals (Dota et al., 2002, 2009; Piotrowskia  
289 and Rozanowski, 2010) can be adapted to detect the events present in LFPs;  
290 however, these algorithms have computational complexities of  $O(n^3)$ .

### 291 4.1. Single experiment

292 The method was applied to a number of datasets and found to be working  
293 quite well except a few situations (2% of occurrence rate) where an error of  
294  $\pm 300 \mu\text{s}$  was noticed in latency calculation. Particularly, latency calculation  
295 error was occurring in case of signals containing slow stimulus artifacts (with  
296 frequency components less than 250 Hz). As latencies are in terms of a  
297 few milliseconds up to hundred of milliseconds, this error can be considered  
298 negligible. Figure 9 shows representative signals and their respective detected  
299 events after a run of the method.

Figure 9: LFP depth profile with detected events using the method mentioned in section 3.1. The signals were recorded equidistantly ( $90 \mu\text{m}$  pitch). For better visualization only representative signals from each layer are shown.

300 When compared, the latency results for the layer activation order ob-  
301 tained from the LFPs and the CSD profile (figure 10 and figure 11) are found  
302 similar in terms of activation sequence, but not with respect to their values.  
303 The layerwise latencies of CSDs are larger than those of the LFPs. This is

304 due to the fact that, in case of the CSDs, latencies are calculated as the dif-  
305 ference between time instance of the first sink's peak and the stimulus-onset,  
306 whereas the latencies for the LFPs are calculated as the difference between  
307 the time instance of the E2 and the stimulus-onset.

Figure 10: Comparison of layer-wise latencies calculated from the LFPs and CSDs.

Figure 11: Layer activation order calculated using the LFP (top) and CSD profiles (bot-  
tom).

308 For determining the layer activation order using CSDs, a common ref-  
309 erence point is required to calculate the latencies, which can be the exact  
310 initiation of the first sink (Kaur et al., 2005; Mitzdorf and Singer, 1980;  
311 Mitzdorf, 1985; Swadlow et al., 2002) or the peak of the first sink (Castro-  
312 Almancos and Oldford, 2002; Di et al., 1990; Megevand et al., 2009; Staba  
313 et al., 2004) or a combination of both (Jellema et al., 2004; Szymanski et  
314 al., 2009). Due to the oscillations in the CSDs caused by calculation, it is  
315 difficult to detect the exact initiation of the first sink in each CSD using an  
316 automated method. Indeed, especially when the LFPs contain high spon-  
317 taneous brain activity or oscillations the generated CSDs are too noisy and  
318 oscillatory. Filtering the LFPs or the CSDs does not really eliminate possi-  
319 bility of miscalculation. Therefore, the difficulty in detecting the first sink's  
320 onset led us to consider the first sink's peak in calculating the latencies. Sci-  
321 entists need to perform the latency calculation manually in cases where a  
322 different reference point is required other than the first sink's peak. To this  
323 respect the method suffers a shortcoming which will require a more complex  
324 algorithm to overcome.

Table 1: Comparison of manual and automatic calculation of latencies

Depth	Mode	Latencies (ms)			
		E1	E2	E3	E4
90 $\mu\text{m}$	M	5.384	19.784	42.934	144.954
	A	5.655	19.564	42.742	143.393
180 $\mu\text{m}$	M	Absent	19.745	60.055	174.215
	A	Absent	19.416	59.259	174.023
270 $\mu\text{m}$	M	Absent	19.905	64.795	180.965
	A	Absent	19.615	63.513	183.733
450 $\mu\text{m}$	M	Absent	20.215	69.395	232.835
	A	Absent	20.228	70.320	232.836
540 $\mu\text{m}$	M	Absent	20.075	74.205	221.595
	A	Absent	20.216	74.124	222.021
720 $\mu\text{m}$	M	Absent	20.645	79.895	283.305
	A	Absent	20.565	78.228	282.532
990 $\mu\text{m}$	M	Absent	19.375	87.805	220.125
	A	Absent	19.464	87.887	175.475
1260 $\mu\text{m}$	M	Absent	18.585	96.025	238.595
	A	Absent	18.213	96.046	239.489
1620 $\mu\text{m}$	M	16.1150	38.925	110.835	202.635
	A	16.116	38.785	112.562	198.448
1800 $\mu\text{m}$	M	10.175	38.585	118.825	234.975
	A	10.310	38.584	118.568	234.784

325 The latencies calculated by the automated method for the LFPs (depth  
326 profile can be seen in figure 9) were also compared with the manually calcu-  
327 lated latencies and the results were found to be similar (table 1). ‘M’ denotes  
328 manual computation by hand and ‘A’ denotes automated calculation using  
329 the method. In table 1 the ‘E1’, ‘E2’, ‘E3’ and ‘E4’ are the latencies of  
330 the respective events. As mentioned in section 2.3 in the upper layers we  
331 can observe the first positive peak, which gradually disappears in the middle  
332 layers and eventually becomes the first negative peak. This phenomena is  
333 also evident in the tables as the latencies of the E1 in the middle layers is re-  
334 ported ‘Absent’. Furthermore, table 2 reports average latencies for 3 different  
335 experiments evaluated manually and by the program with their root mean  
336 square errors (RMSE). In table 2 the ‘E1’, ‘E2’, ‘E3’ and ‘E4’ are averaged  
337 latencies and RMSE of the respective events. The low RMSE indicates that  
338 the calculation of latencies using the automated method is accurate. The  
339 tables report data corresponding to representative signal(s) from depth(s) of  
340 each layer (please see figure 9).

Table 2: Average latencies of events using manual and automatic calculation with RMSE

Depth	Mode	Average Latencies (ms)				RMS Errors			
		E1	E2	E3	E4	E1	E2	E3	E4
90 $\mu\text{m}$	M	6.019	19.784	42.450	139.014	0.542	0.081	0.024	0.315
	A	6.592	19.564	42.201	140.047				
180 $\mu\text{m}$	M	Absent	19.745	67.547	178.850	Absent	0.092	0.021	0.221
	A	Absent	19.416	68.974	175.654				
270 $\mu\text{m}$	M	Absent	28.517	62.574	183.015	Absent	0.026	0.032	0.254
	A	Absent	28.428	65.051	187.373				
450 $\mu\text{m}$	M	Absent	25.591	74.102	221.301	Absent	0.062	0.028	0.253
	A	Absent	25.675	77.108	203.952				
540 $\mu\text{m}$	M	Absent	18.175	71.214	231.595	Absent	0.059	0.046	0.477
	A	Absent	18.318	72.980	213.741				
720 $\mu\text{m}$	M	Absent	20.145	72.985	210.745	Absent	0.048	0.094	0.351
	A	Absent	19.619	73.428	271.659				
990 $\mu\text{m}$	M	Absent	21.937	84.862	192.251	Absent	0.095	0.392	0.853
	A	Absent	22.121	90.957	183.241				
1260 $\mu\text{m}$	M	Absent	18.985	91.213	210.021	Absent	0.036	0.095	0.764
	A	Absent	19.018	91.478	228.674				
1620 $\mu\text{m}$	M	11.152	26.132	110.835	192.380	0.152	0.071	0.93	0.429
	A	10.920	25.925	112.562	181.154				
1800 $\mu\text{m}$	M	9.631	35.585	117.241	221.341	0.821	0.087	0.034	0.762
	A	9.927	35.885	113.231	214.114				

341 Also, activation orders of cortical layers based on manual calculation and  
 342 by the method are exactly the same (figure 12). Therefore, results of table 1,  
 343 2 and figure 12 suggest that the automated method is accurate in detecting  
 344 the various events present in the LFPs and in calculating latencies with  
 345 precisions that are sufficient for a reliable determination of the activation  
 346 order of cortical layers.

Figure 12: Comparison of manual and automatic method's latency calculation in finding the activation order of different cortical layers.

347 In conclusion, basing on these evidences, we can assert that the automated  
 348 method presented can calculate the activation order of layers in the barrel  
 349 columns upon mechanical whisker stimulation in a single experiment. Both  
 350 the approaches (using LFP or CSD) provide similar results; it is the choice  
 351 of the user to decide which one to use based on the need.

#### 352 4.2. Average across experiments

353 In addition to the single experiments we also applied our method to the  
 354 grand average across three different experiments. This type of averaging  
 355 technique has been adopted by previous studies to determine the temporal  
 356 order of layer activation in the cortex (Di et al., 1990; Jellema et al., 2004;  
 357 Staba et al., 2004). During these experiments, the signals are recorded at a

358 pitch of 90  $\mu\text{m}$  by mechanically stimulating the D1 whisker. Thus, the signals  
359 were averaged across experiments (depthwise) to obtain a grand average LFP  
360 profile. This profile was then used to calculate the layer activation order using  
361 LFPs and CSDs.

362 To obtain the layer activation order from the grand average LFPs, the  
363 latencies of different events (E1–E4) were calculated and grouped layerwise.  
364 The minimum latency in each layer was found and sorted in ascending order,  
365 thus providing the activation order. The CSD profile was calculated using the  
366 grand average LFP profile through application of  $\delta$ -iCSD method. Latencies  
367 were calculated considering the first sink's peak and were grouped layerwise.  
368 The minimum latency in each layer was found and sorted in ascending order  
369 to obtain the activation order.

370 Figure 13 shows the latencies obtained from the grand average LFP profile  
371 and the CSD profile obtained using the  $\delta$ -iCSD method. Standard deviations  
372 of the means are shown as vertical bars. The latencies at different depths  
373 obtained using the grand average by the two methods show a temporal order  
374 of layer excitation comparable to previous studies (Armstrong-James et al.,  
375 1992; Di et al., 1990; Einevoll et al., 2007).

Figure 13: Latencies obtained from the grand average (n=3). Latencies calculated using LFP based method (top) and latencies calculated using CSD based method (bottom). The vertical bars show standard deviations of the means.

## 376 5. Conclusion

377 Whisking in the rodents is one of the most important ways in exploring  
378 the environments. To understand the whisking mechanism, its role in lo-  
379 calizing objects and discriminate among them based on shape and texture  
380 are under extensive study. To perform this kind of studies, determining the  
381 signal processing pathway and, in turn, the order of activation of different  
382 cortical layers is very important. Scientists perform this task manually which  
383 is time consuming and boring. As evidenced above, the proposed method is  
384 an automated solution in performing this kind of analysis. Two methods  
385 are automated, one uses the LFPs and the other one the CSDs. Depend-  
386 ing on the need, the user can select either of them and have a qualitative  
387 assessment of the layer activation order. Moreover, the method using LFPs  
388 is computationally efficient, quick and easy to implement. As it involves  
389 less calculations compared to the CSD based approach, this method could

390 be preferably adapted for analysis of signals recorded using high resolution  
391 brain–chip interfaces or neural probes capable of recording large amounts of  
392 data during an experiment. This layer activation order detection toolbox is  
393 a part of the SigMate software package that will be made available to the  
394 community shortly (Mahmud et al., 2010b).

395

## 396 **Acknowledgment**

397

398 This work was carried out as a part of the European Commission funded  
399 CyberRat project under the Seventh Framework Programme (ICT-2007.8.3  
400 Bio-ICT convergence, 216528, CyberRat).

401

## 402 **References**

- 403 Ahissar E, Knutsen KM. Object localization with whiskers. *Biol Cybern* 2008; 98(6):449–58.  
404
- 405 Ahrens KF, Kleinfeld D. Current flow in vibrissa motor cortex can phase-lock with exploratory rhythmic  
406 whisking in rat. *J Neurophysiol*, 2004; 92:1700–7.  
407
- 408 Alloway KD. Information processing streams in rodent barrel cortex: the differential functions of barrel  
409 and septal circuits. *Cereb Cortex*, 2008; 18(5):979–98.  
410
- 411 Armstrong-James M, Fox K, Das-Gupta A. Flow of excitation within rat barrel cortex on striking a single  
412 vibrissa. *J Neurophysiol* 1992; 68(4):1345–57.  
413
- 414 Bokil HS, Pesaran B, Andersen RA, Mitra PP. A method for detection and classification of events in  
415 neural activity. *IEEE T Bio-Med Eng*, 2006; 53(8): 1678–87.  
416
- 417 Brett-Green BA, Chen-Bee CH, Frostig RD. Comparing the functional representations of central and border  
418 whiskers in rat primary somatosensory cortex. *J Neurosci*, 2001; 21(24):9944–54.  
419
- 420 Castro-Alamancos MA, Oldford E. Cortical sensory suppression during arousal is due to the activity-  
421 dependent depression of thalamocortical synapses. *J Physiol*, 2002; 541(1): 319–31.  
422
- 423 Di S, Baumgartner C, Barth D S. Laminar Analysis of extracellular field potentials in rat vibrissa/barrel  
424 cortex. *J Neurophysiol*, 1990; 63: 832–40.  
425
- 426 Diamond ME, vo Heimendahl M, Knutsehn PM, Kleinfeld D, Ahissar D. ‘Where’ and ‘what’ in the whisker  
427 sensorimotor system. *Nat Rev Neurosci*, 2008; 9:601–12.  
428
- 429 Dota C, Skallefoll B, Edvardsson N, Fager G. Computer-based analysis of dynamic QT changes: toward  
430 high precision and individual rate correction. *Ann Noninvas Electro*, 2002; 7(4): 289–301.  
431
- 432 Dota CD, Edvardsson N, Skallefoll B, Fager G. PC-based ECG waveform recognition/validation of novel  
433 software against a reference ECG database. *Ann Noninvas Electro*, 2009; 14(1): S42-7.  
434
- 435 Einevoll GT, Pettersen KH, Devor A, Ulbert I, Halgren E, Dale AM. Laminar population analysis: es-  
436 timating firing rates and evoked synaptic activity from multielectrode recordings in rat barrel cortex. *J*  
437 *Neurophysiol* 2007; 97:2174–90.  
438
- 439 Fox K. *Barrel Cortex*. Cambridge: Cambridge University Press; 2008.  
440

441 Jellema T, Brunia CHM, Wadman WJ. Sequential activation of microcircuits underlying somatosensory-  
442 evoked potentials in rat neocortex. *Neuroscience*, 2004; 129: 283–95.  
443

444 Kaur S, Rose H J, Lazar R, Liang K, Metherate R. Spectral integration in primary auditory cortex: lam-  
445 inar processing of afferent input, in vivo and in vitro. *Neuroscience*, 2005; 134: 1033–45.  
446

447 Kublik E. Contextual impact on sensory processing at the barrel cortex of awake rat. *Acta Neurobiol*  
448 *Exp*, 2004; 64:229–38.  
449

450 Mahmud M, Bertoldo A, Maschietto M, Girardi S, Vassanelli S. Automatic detection of layer activation  
451 order in information processing pathways of rat barrel cortex under mechanical whisker stimulation. In:  
452 Proc. of the 32nd annual international conference of the IEEE engineering in medicine and biology society  
453 (IEEE EMBC2010); 2010a. p. 6095–8.  
454

455 Mahmud M, Bertoldo A, Girardi S, Maschietto M, Vassanelli S. SigMate: a MATLAB-based neuronal  
456 signal processing tool. In: Proc. of the 32nd annual international conference of the IEEE engineering in  
457 medicine and biology society (IEEE EMBC2010); 2010b. p. 1352–5.  
458

459 Megevand P, Troncoso E, Quairiaux C, Muller D, Michel CM, Kiss JZ. Long-term plasticity in mouse  
460 sensorimotor circuits after rhythmic whisker stimulation. *J Neurosci*, 2009; 29(16): 5326–35.  
461

462 Mitzdorf U, Singer W. Monocular activation of visual cortex in normal and monocularly deprived cats:  
463 an analysis of evoked potentials. *J Physiol*, 1980; 304: 203–20.  
464

465 Mitzdorf U. Current source-density method and application in cat cerebral cortex: investigation of evoked  
466 potentials and EEG phenomena. *Physiol Rev*, 1985; 65: 37–100.  
467

468 Pettersen KH, Devor A, Ulbert I, Dale AM, Einevoll GT. Current-source density estimation based on  
469 inversion of electrostatic forward solution: Effects of finite extent of neuronal activity and conductivity  
470 discontinuities. *J Neurosci Meth*, 2006; 154:116–33.  
471

472 Piotrowskia Z, Rozanowski K. Robust algorithm for heart rate (HR) detection and heart rate variability  
473 (HRV) estimation. *Acta Physica Polonica A*, 2010; 118(1): 131–5.  
474

475 Rappelsberger P, Pockberger H, Petsche H. Current source density analysis: methods and application to  
476 simultaneously recorded field potentials of the rabbit's visual cortex. *Pflugers Arch*, 1981; 389:159–70.  
477

478 Schubert D, Kotter R, Staiger JF. Mapping functional connectivity in barrel-related columns reveals  
479 layer- and cell type-specific microcircuits. *Brain Struct Funct*, 2007; 212:107–19.  
480

481 Sekino M, Ohsaki H, Yamaguchi-Sekino S, Iriguchi N, Ueno S. Low-frequency conductivity tensor of rat  
482 brain tissues inferred from diffusion mri. *Bioelectromagnetics*, 2009; 30(6):489–99.  
483

484 Staba RJ, Bergmann PC, Barth DS. Dissociation of slow waves and fast oscillations above 200 Hz during  
485 GABA application in rat somatosensory cortex. *J Physiol*, 2004; 561(1): 205–14.  
486

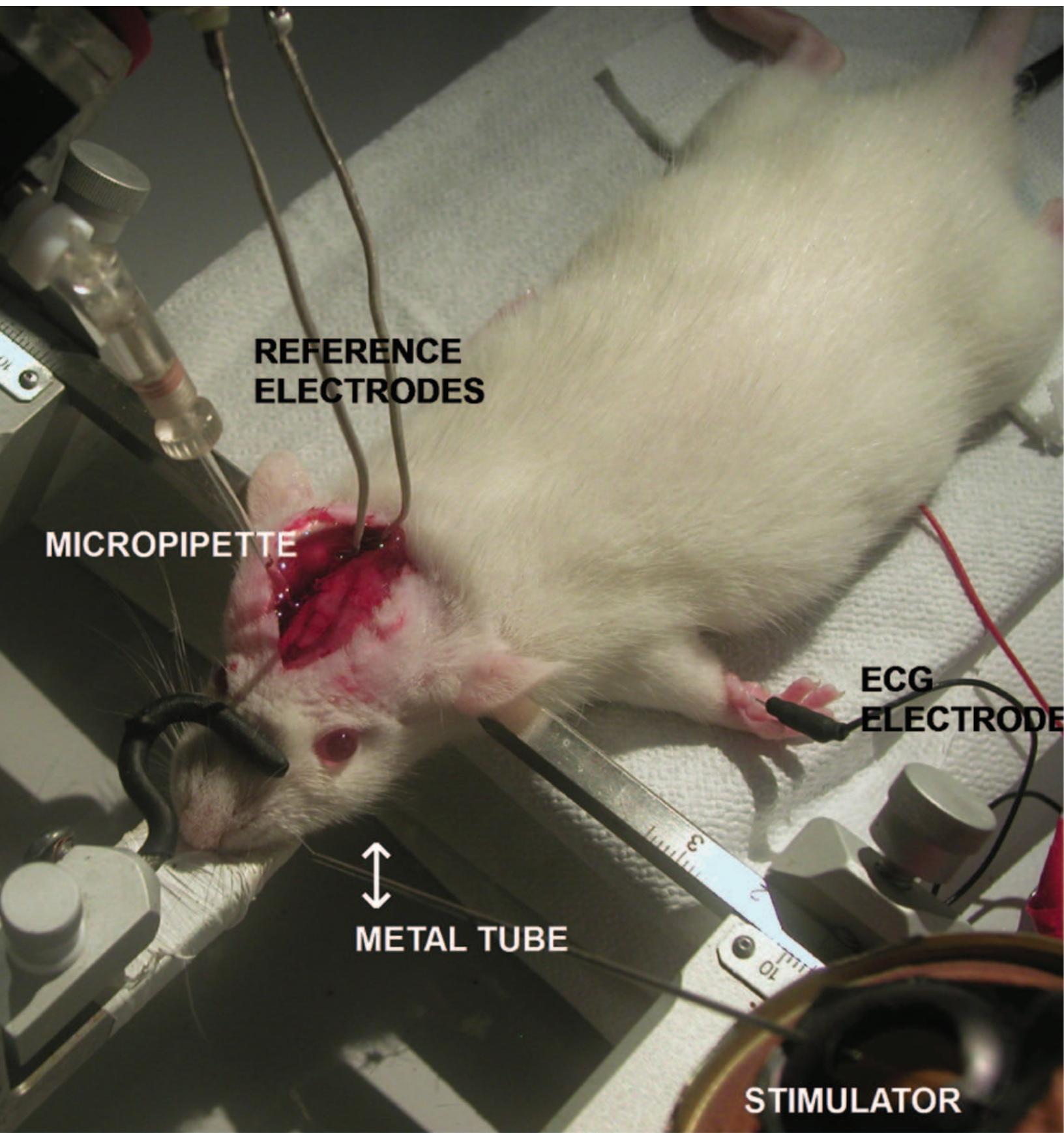
487 Swadlow H A, Gusev A G, Bezdudnaya T. Activation of a cortical column by a thalamocortical impulse.  
488 *J Neurosci*, 2002; 22(17): 7766–73.  
489

490 Swanson LW. *Brain Maps: Structure of the Rat Brain*, third ed. London: Academic Press; 2003.  
491

492 Szymanski FD, Garcia-Lazaro JA, Schnupp JWH. Current source density profiles of stimulus-specific  
493 adaptation in rat auditory cortex. *J Neurophysiol*, 2009; 102:1483–90.  
494

495 Ulbert I, Karmos G, Heit G, Halgren E. Early discrimination of coherent versus incoherent motion by  
496 multiunit and synaptic activity in human putative MT+. *Hum Brain Mapp*, 2001; 13: 226–38.  
497

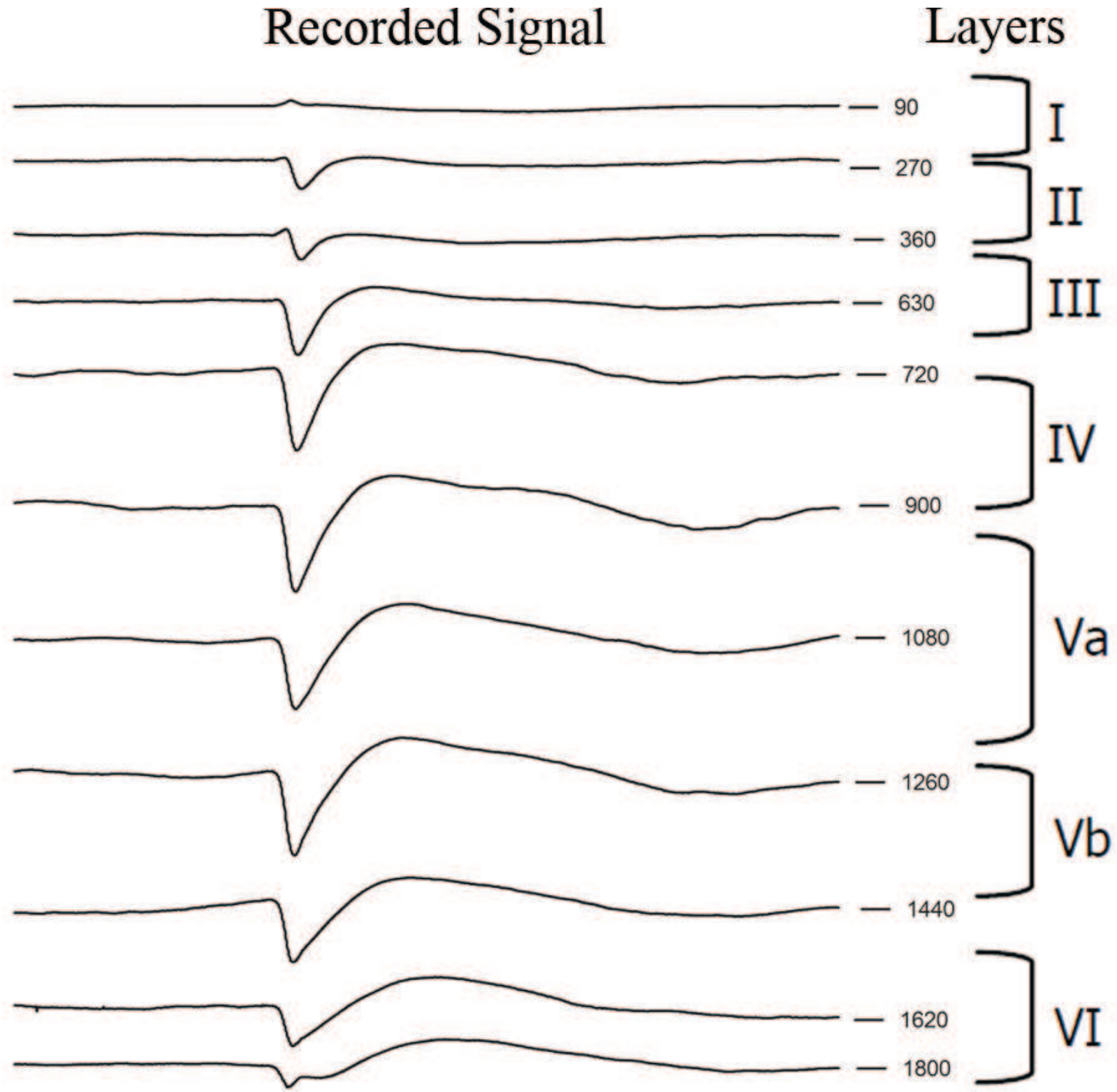
Figure 1



1 ms  
10V

150 ms

Figure 2



Cite as: Mahmud, M., Pasqualotto, E., Bertoldo, A., Girardi, S., Maschietto, M., Vassanelli, S. An automated method for detection of layer activation order in information processing pathway of rat barrel cortex under mechanical whisker stimulation. (2011) Journal of Neuroscience Methods, 196 (1), pp. 141-150. doi: 10.1016/j.jneumeth.2010.11.024  
Copyright © 2011 Elsevier B.V. All rights reserved.

0.5 mV  
100 ms  
stim

Figure 3

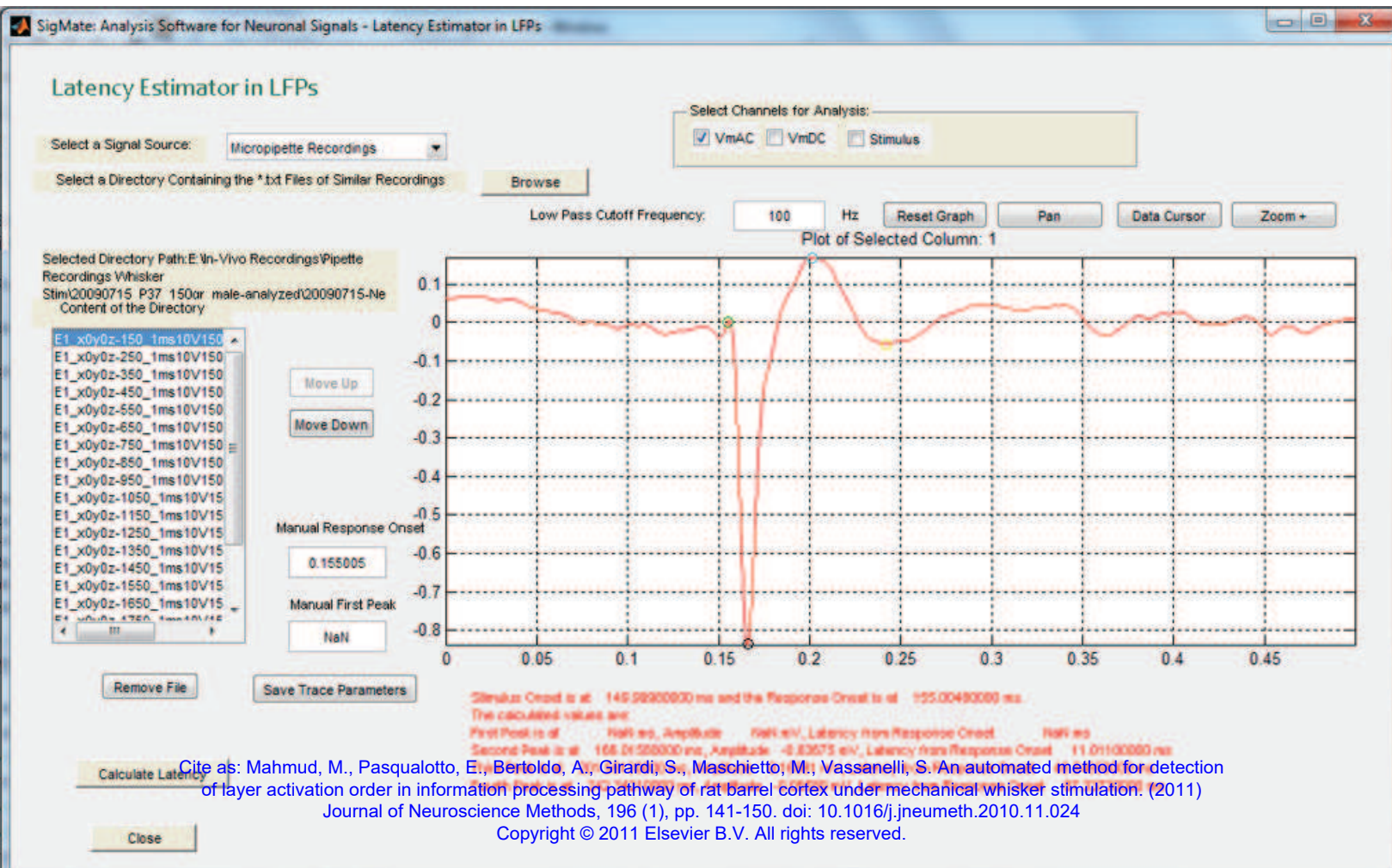


Figure 4

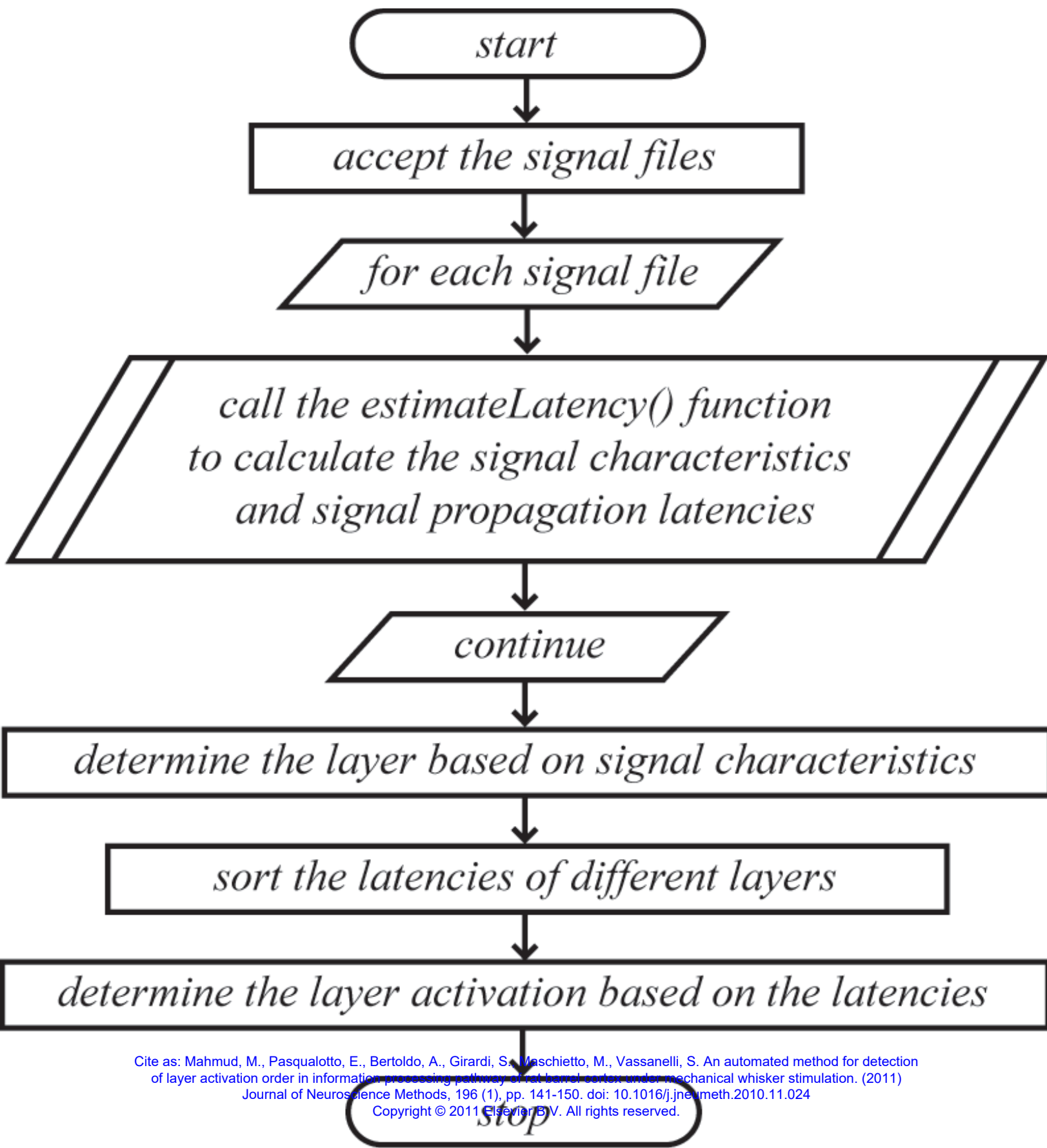
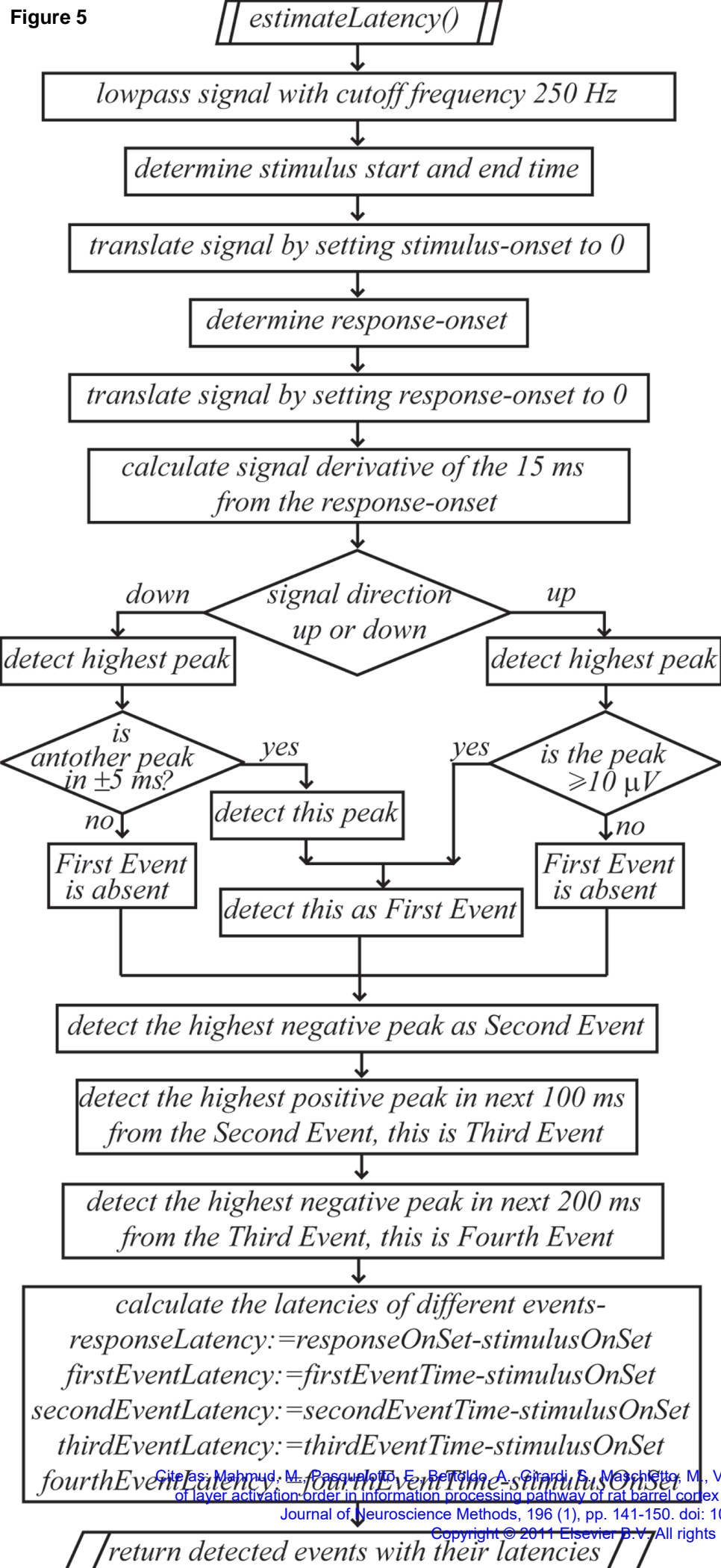


Figure 5

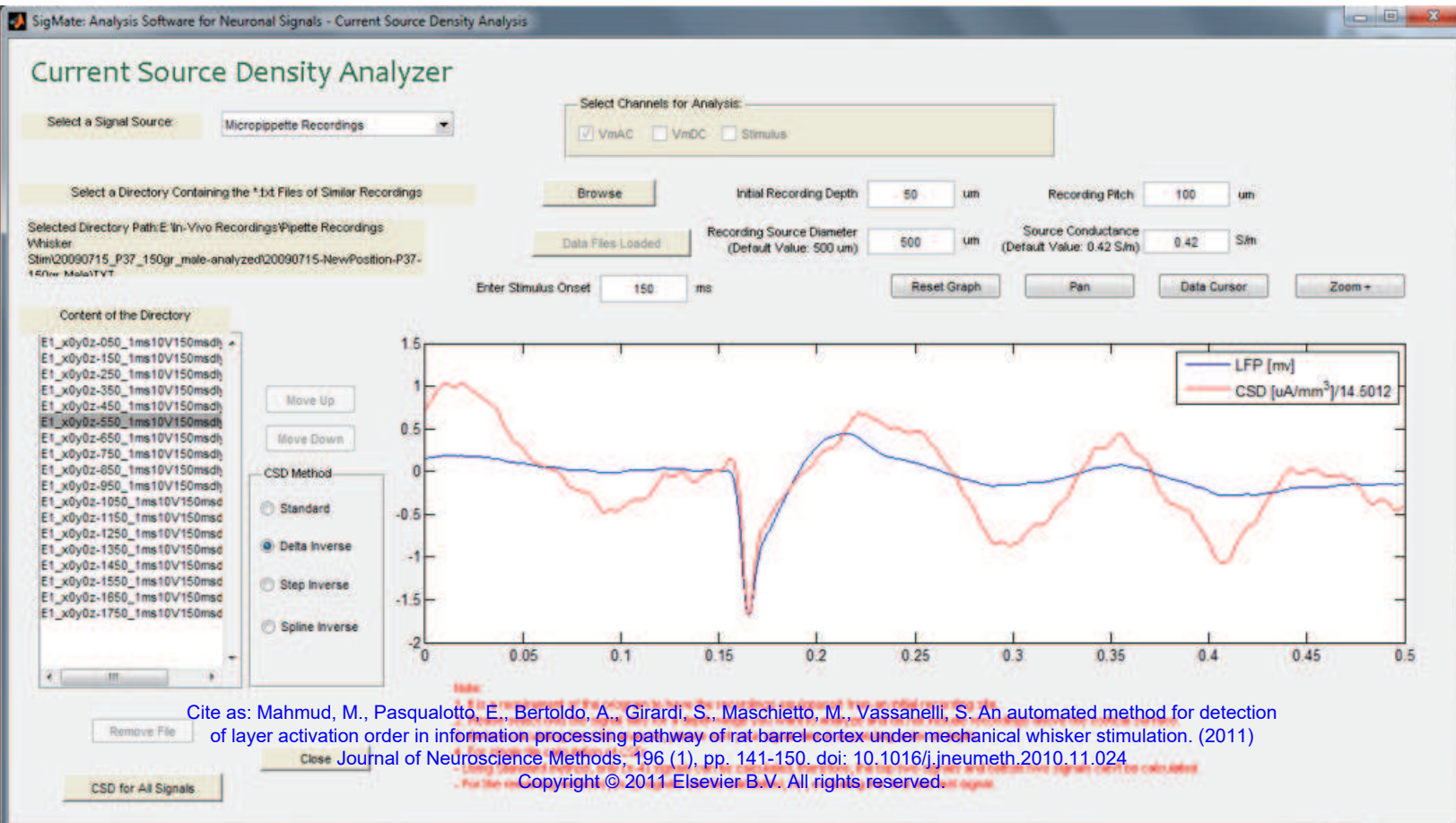


Cite as: Mahmud, M., Pasqualito, E., Berglido, A., Girardi, S., Maschitto, M., Vassanelli, S. An automated method for detection of layer activation order in information processing pathway of rat barrel cortex under mechanical whisker stimulation. (2011)

Journal of Neuroscience Methods, 196 (1), pp. 141-150. doi: 10.1016/j.jneumeth.2010.11.024

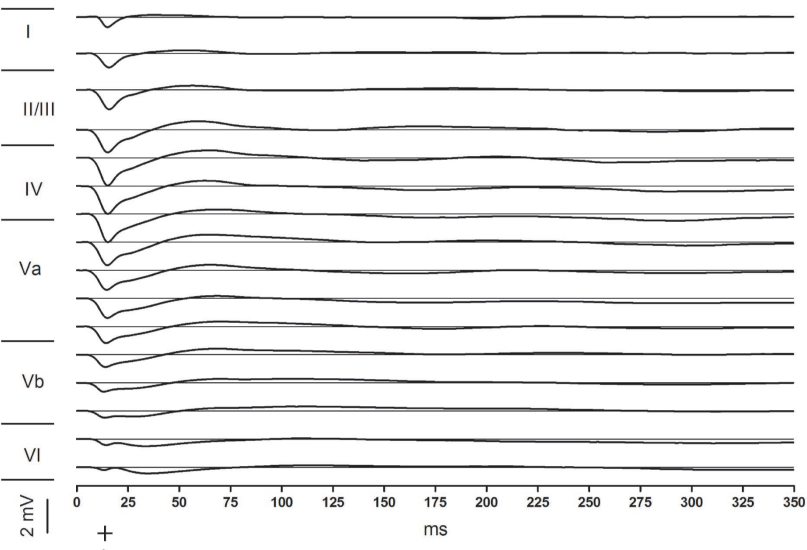
Copyright © 2011 Elsevier B.V. All rights reserved.

Figure 6

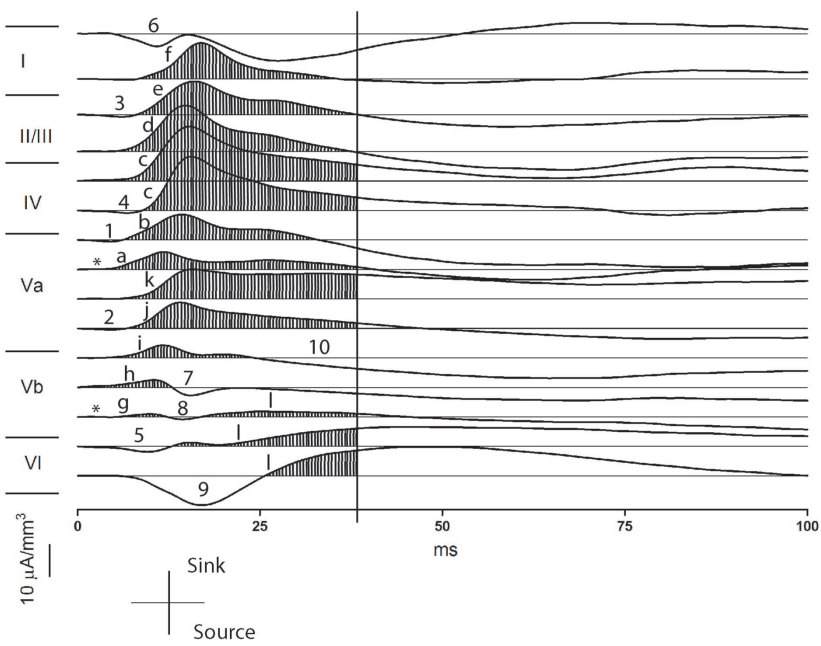


**Figure 7**

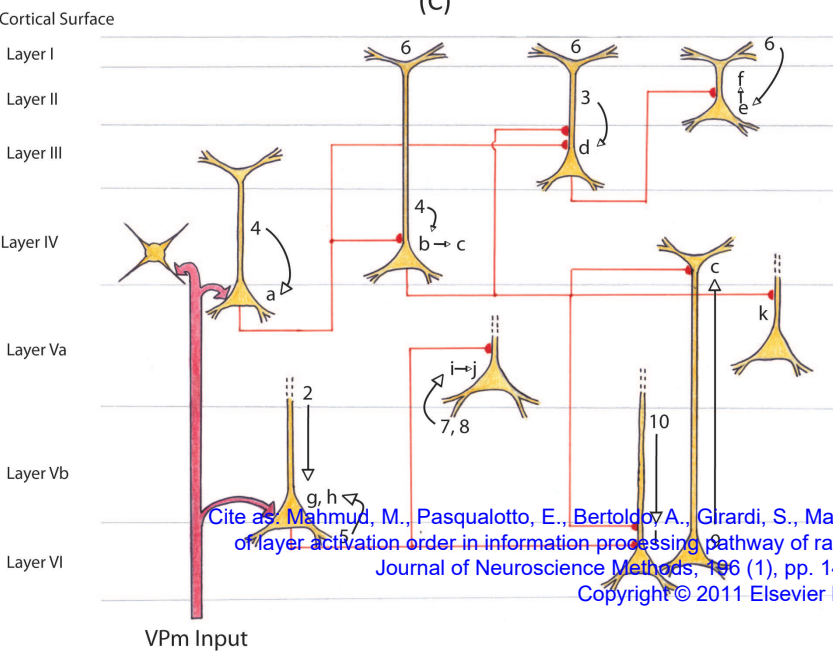
**Local Field Potential Recorded from S1**



**(B)**  
**CSD using Delta iCSD Method**



**(C)**

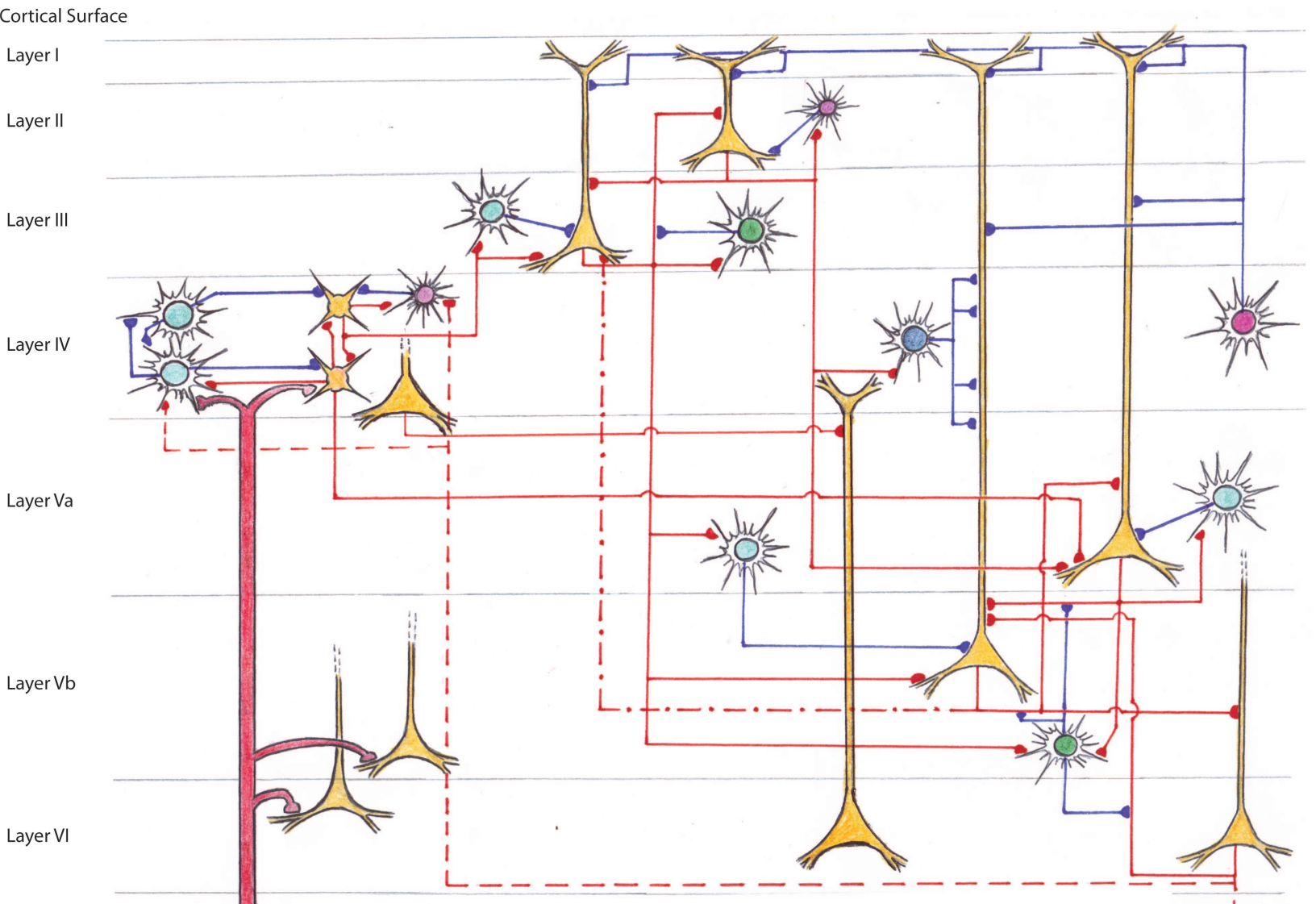


Cite as: Mahmud, M., Pasqualotto, E., Bertoldo A., Girardi, S., Maschietto, M., Vassanelli, S. An automated method for detection of layer activation order in information processing pathway of rat barrel cortex under mechanical whisker stimulation. (2011) Journal of Neuroscience Methods, 196 (1), pp. 141-150. doi: 10.1016/j.jneumeth.2010.11.024

Copyright © 2011 Elsevier B.V. All rights reserved.

Figure 8

### Barrel Cortex Architecture



### Legend

- 

Stellate Cells
- 

Low Threshold Spiking Cells
- 

Martinotti Cells
- 

Pyramidal Cells
- 

Chandelier Cells
- 

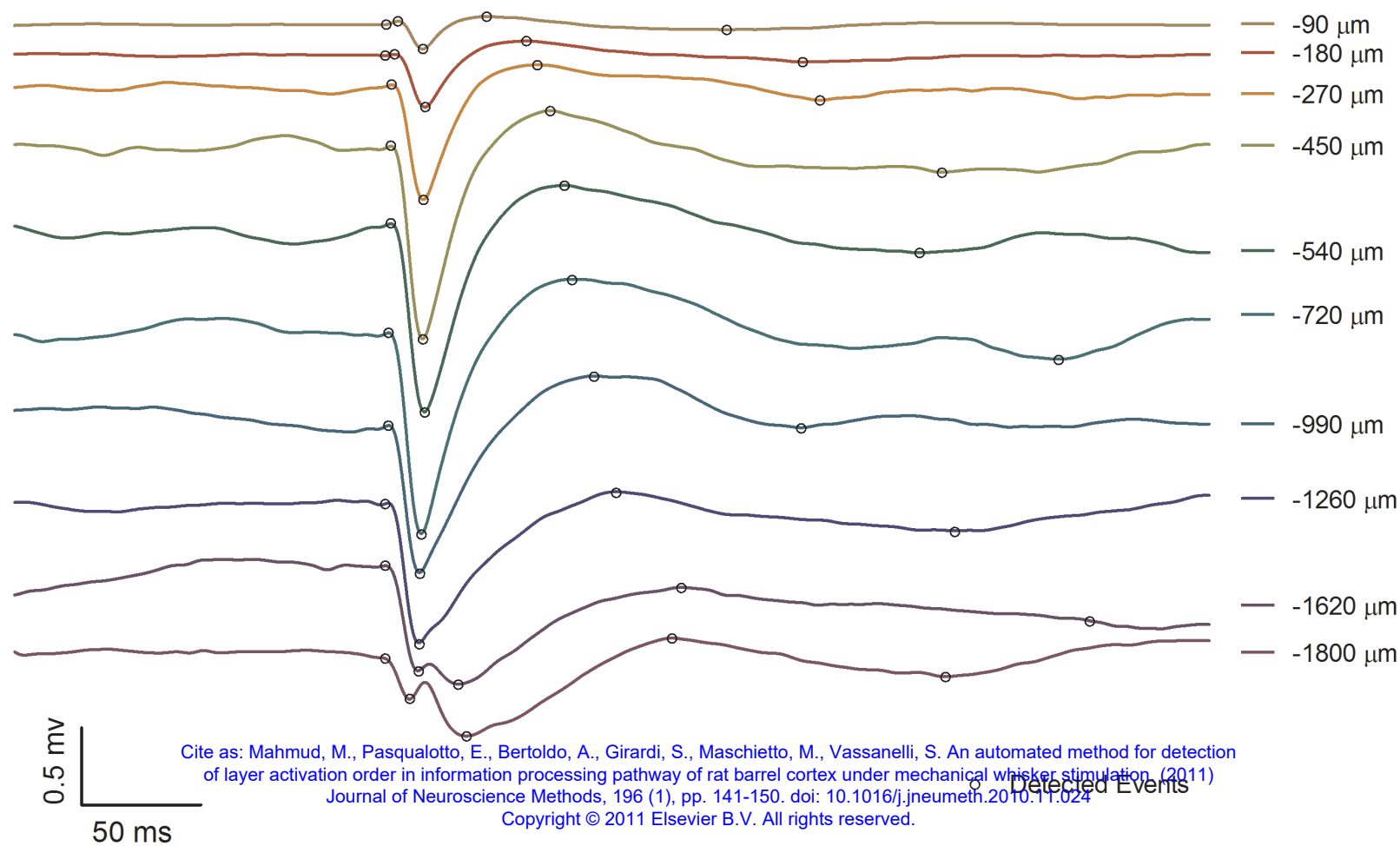
Basket Cells

Cite as: Mahmud, M., Pasqualotto, E., Bertolo, A., Girardi, G., Maschietto, M., Vassanelli, S. An automated method for detection of layer activation order in information processing pathway of rat barrel cortex under mechanical whisker stimulation (2011) Journal of Neuroscience Methods, 196 (1), pp. 141-150. doi: 10.1016/j.jneumeth.2010.11.024  
 Copyright © 2011 Elsevier B.V. All rights reserved.

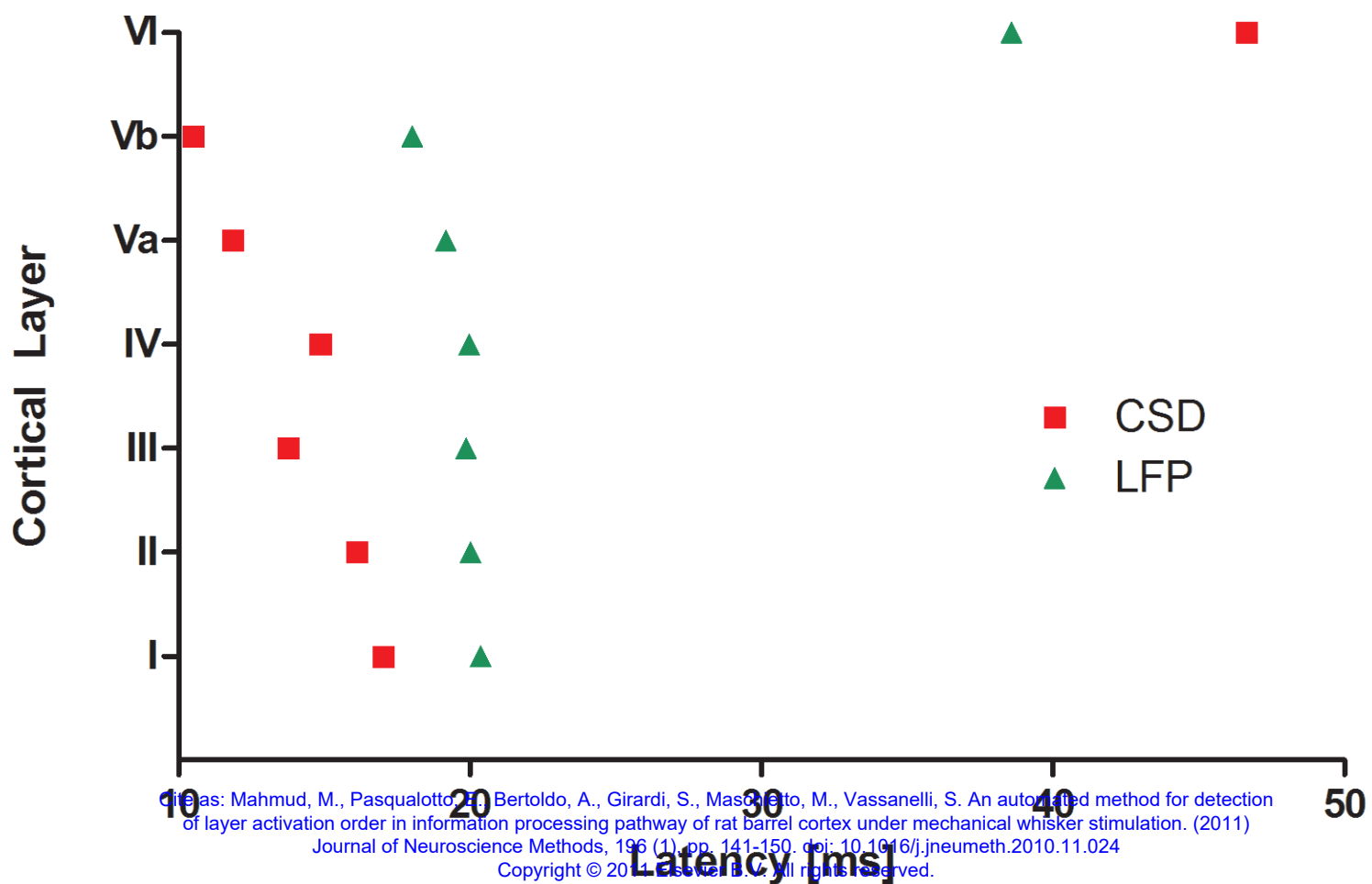
Excitatory Connection  
 Inhibitory Connection  
 Feedback Connection from Layer V to Layer III  
 Feedback Connection to Inhibitory Cells

Figure 9

### Detected Events of LFPs at Different Depths Recorded from the D1 Barrel

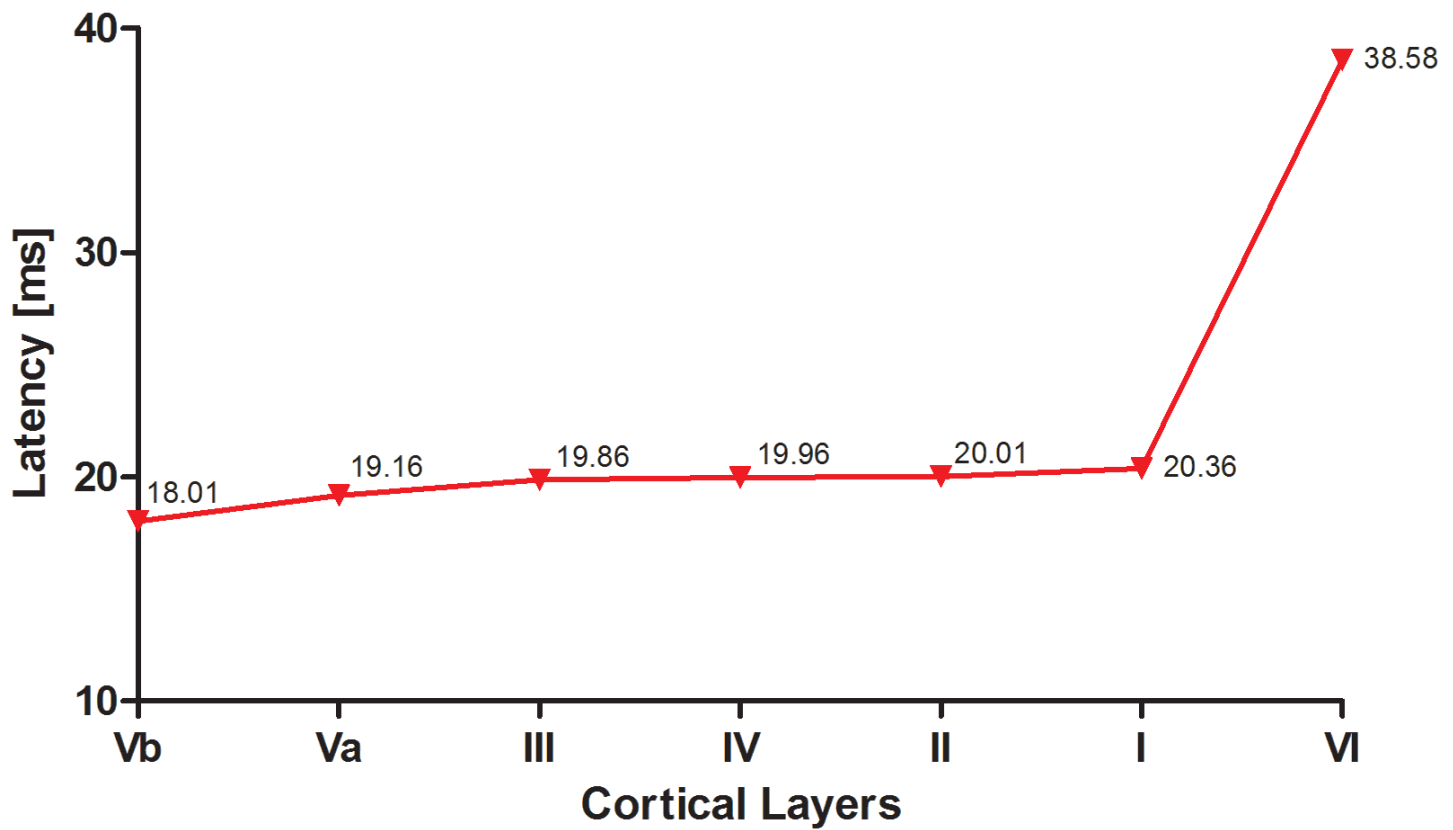


### Latencies Calculated using LFP and CSD

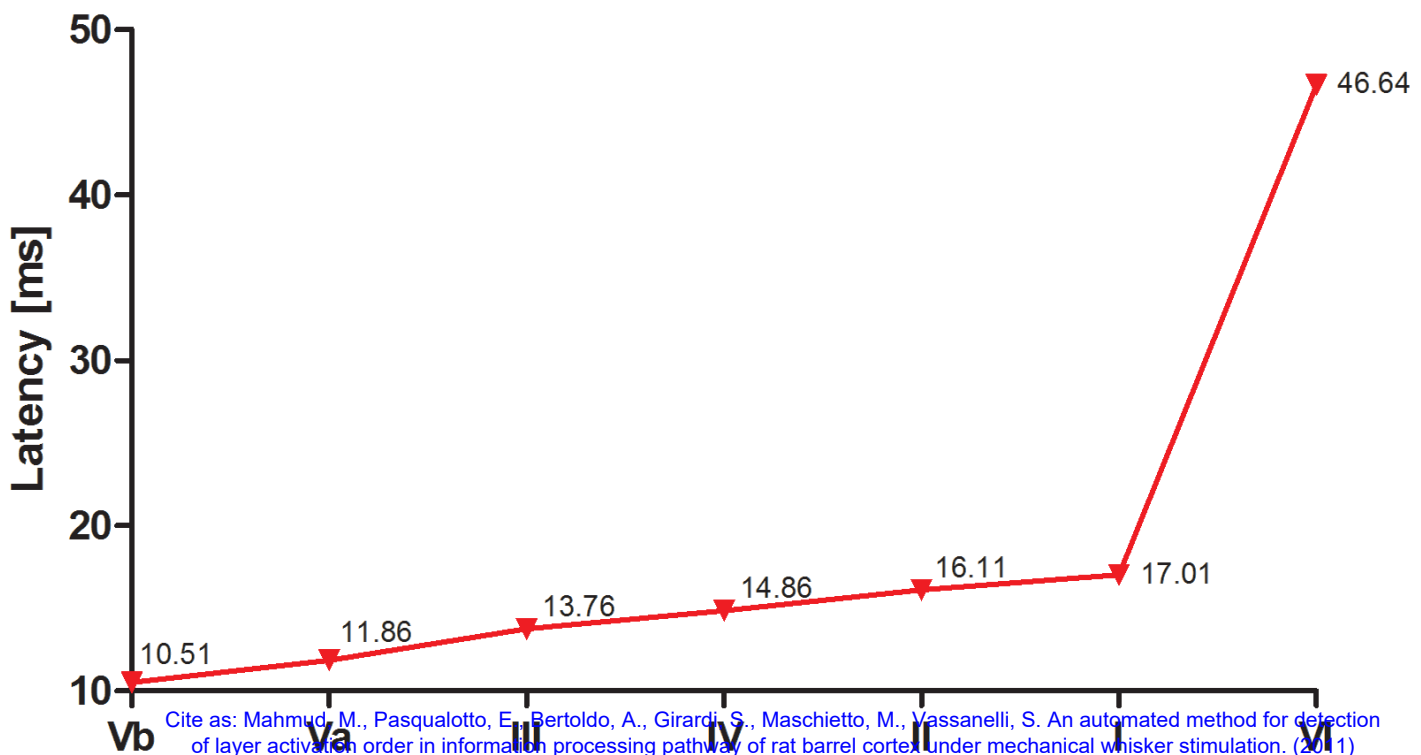


Cite as: Mahmud, M., Pasqualotto, F., Bertoldo, A., Girardi, S., Masciullo, M., Vassanelli, S. An automated method for detection of layer activation order in information processing pathway of rat barrel cortex under mechanical whisker stimulation. (2011) Journal of Neuroscience Methods, 196 (1), pp. 141-150. doi: 10.1016/j.jneumeth.2010.11.024  
Copyright © 2011 Elsevier B.V. All rights reserved.

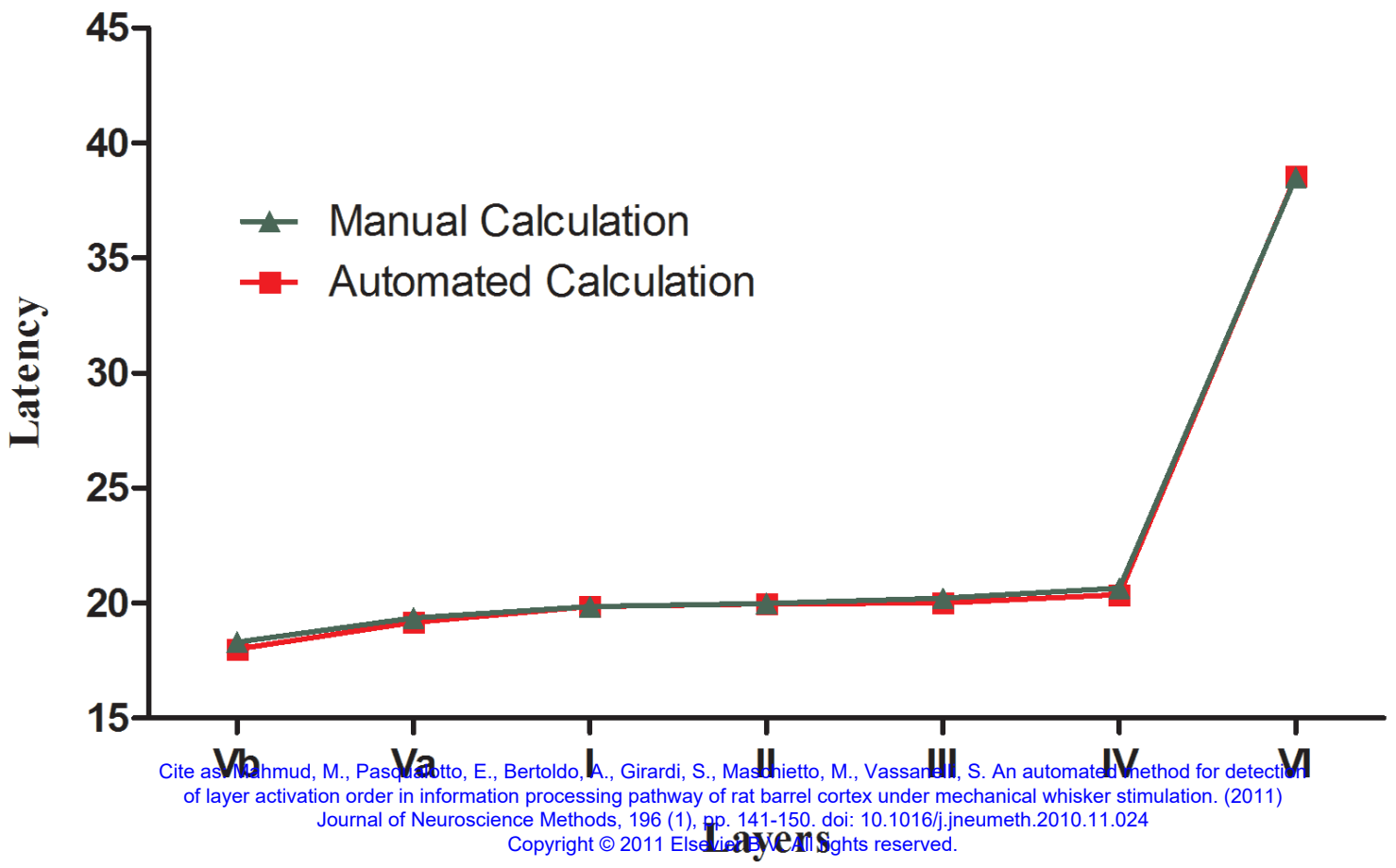
## Layer Activation Order with LFP



## Layer Activation Order with CSD



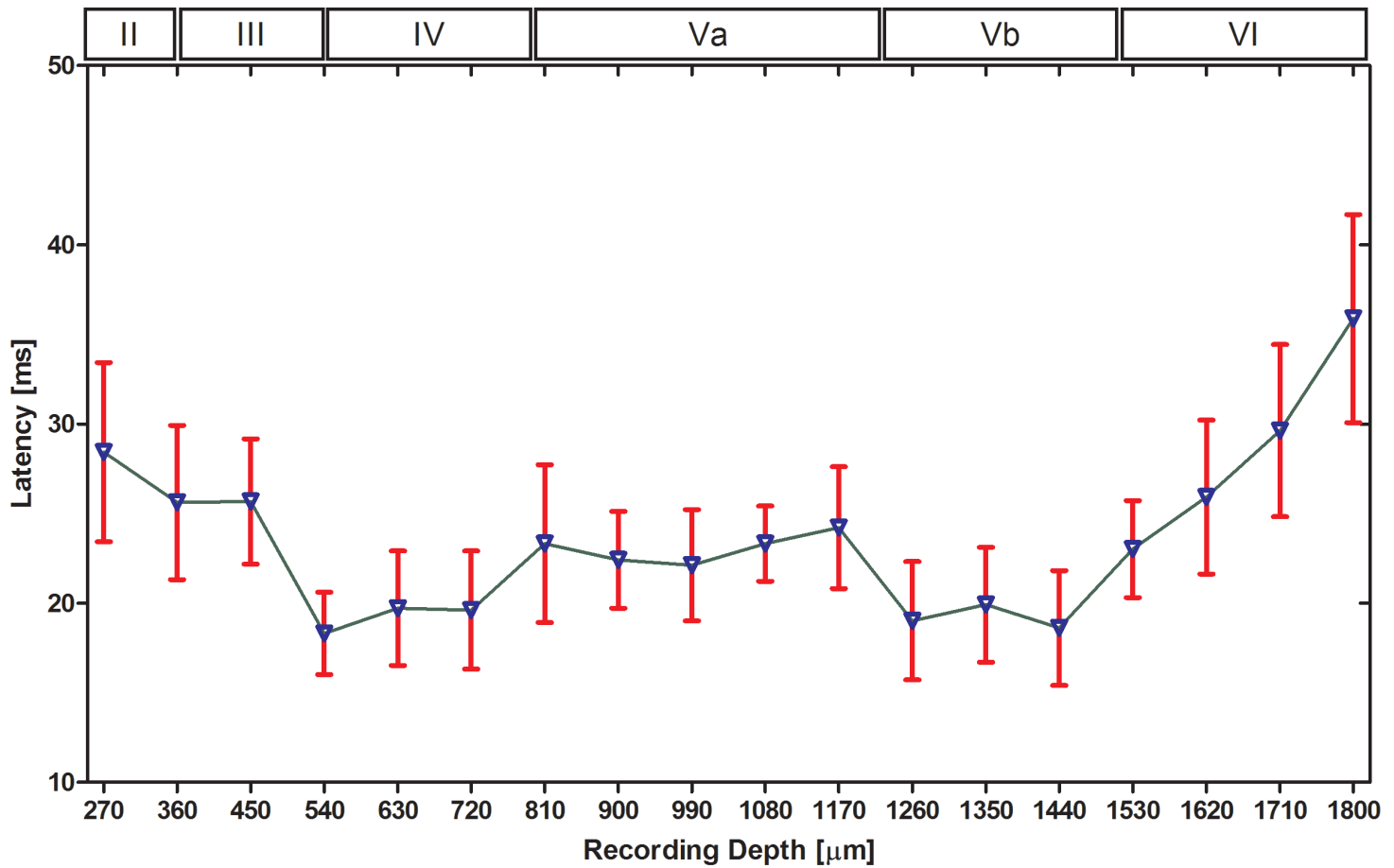
### Comparison of Barrel Cortex Layer Activation



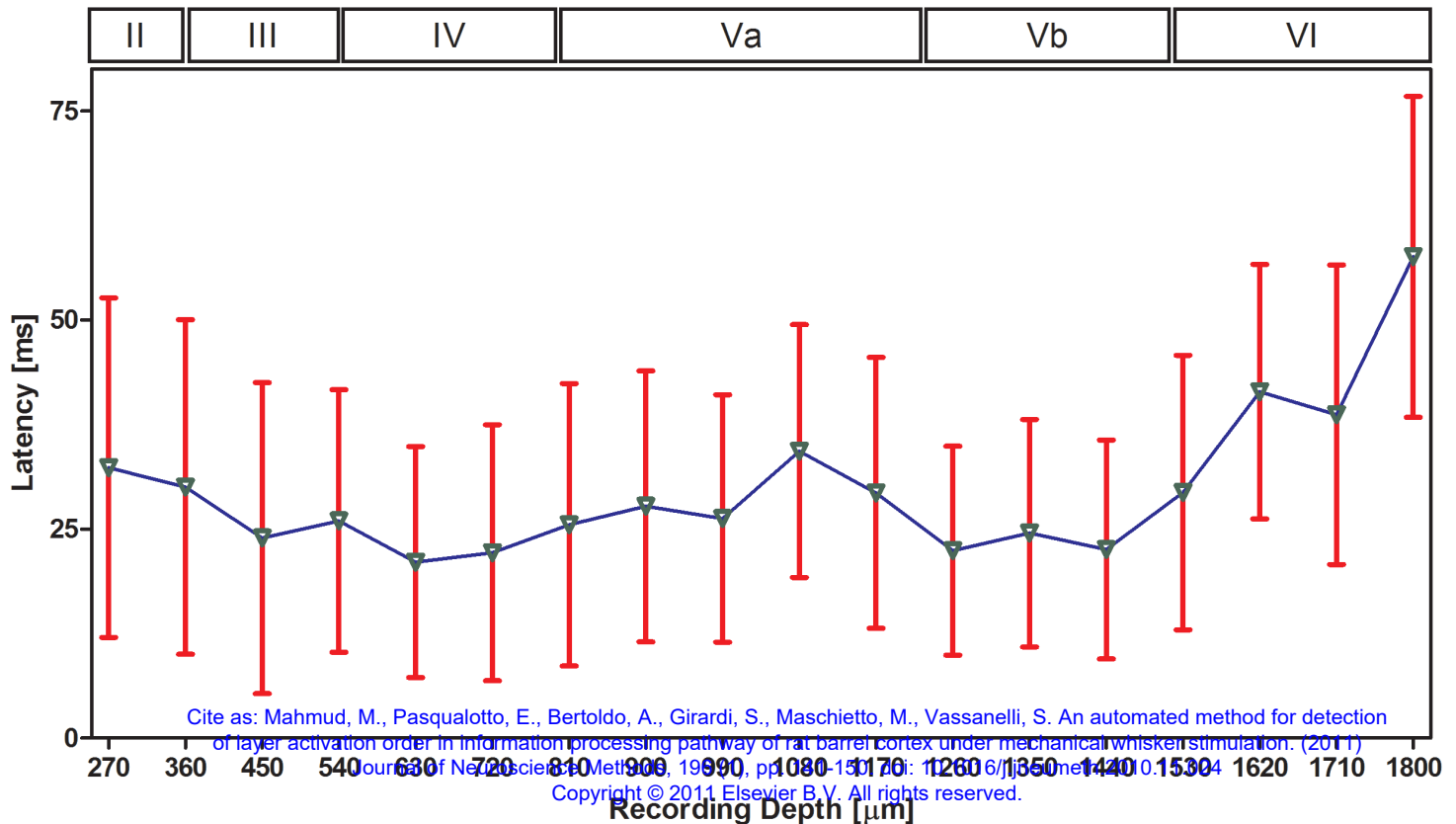
Cite as: Mahmud, M., Pasquotto, E., Bertoldo, A., Girardi, S., Maschietto, M., Vassarelli, S. An automated method for detection of layer activation order in information processing pathway of rat barrel cortex under mechanical whisker stimulation. (2011) Journal of Neuroscience Methods, 196 (1), pp. 141-150. doi: 10.1016/j.jneumeth.2010.11.024  
Copyright © 2011 Elsevier B.V. All rights reserved.

Figure 13

### Latency from Grand Average LFP Profile



### Latency in CSD Profile Obtained from Grand Average LFP Profile



Cite as: Mahmud, M., Pasqualotto, E., Bertoldo, A., Girardi, S., Maschietto, M., Vassanelli, S. An automated method for detection of layer activation order in information processing pathway of rat barrel cortex under mechanical whisker stimulation. (2011)

Journal of Neuroscience Methods, 199, pp. 1-15. doi: 10.1016/j.jneumeth.2010.10.004

Copyright © 2011 Elsevier B.V. All rights reserved.